Current-Temperature Scaling for a Schottky Interface with Nonparabolic Energy Dispersion

Y. S. Ang* and L. K. Ang†

SUTD-MIT International Design Center, Singapore University of Technology and Design, Singapore 487372, Singapore and Engineering Product Development, Singapore University of Technology and Design, Singapore 487372, Singapore

(Received 7 June 2016; revised manuscript received 21 June 2016; published 21 September 2016)

In this paper, we study the Schottky transport in a narrow-gap semiconductor and few-layer graphene in which the energy dispersions are highly nonparabolic. We propose that the contrasting current-temperature scaling relation of $J \propto T^2$ in the conventional Schottky interface and $J \propto T^3$ in graphene-based Schottky interface can be reconciled under Kane's $\mathbf{k} \cdot \mathbf{p}$ nonparabolic band model for narrow-gap semiconductors. Our model suggests a more general form of $J \propto (T^2 + \gamma k_B T^3)$, where the nonparabolicty parameter γ provides a smooth transition from T^2 to T^3 scaling. For few-layer graphene, we find that N-layer graphene with ABC stacking follows $J \propto T^{2/N+1}$, while ABA stacking follows a universal form of $J \propto T^3$ regardless of the number of layers. Intriguingly, the Richardson constant extracted from the Arrhenius plot using an incorrect scaling relation disagrees with the actual value by 2 orders of magnitude, suggesting that correct models must be used in order to extract important properties for many Schottky devices.

DOI: 10.1103/PhysRevApplied.6.034013

I. INTRODUCTION

Translating the unusual physical properties of nanomaterial-based heterostructures into functional device applications has become one of the major research goals in recent years [1]. One important heterostructure is the metal-semiconductor interface, commonly known as the *Schottky interface* [2], where applications such as broadband ultrasensitive photodetectors [3], gate-tunable Schottky barriers [4], promising solar-cell performance [5], and ultrafast phototransistors [6] have recently been demonstrated. The current transport across a Schottky interface is mainly due to majority carriers. In general, there are three different transport mechanisms, namely, diffusion of carriers from the semiconductor into the metal, thermionic emission of carriers across the Schottky barrier, and quantum-mechanical tunneling through the barrier [7]. For the thermionic emission, the Schottky-diode equation is written as [8]

$$J = \overline{J}[e^{(\mathrm{eV}/\eta k_B T)} - 1], \tag{1}$$

where $\overline{J}$ is the reverse saturation current density determined by the thermionic emission process, V is the bias voltage, and η is an ideality factor. For bulk materials with parabolic energy dispersion ($E_k \propto k^2$), the reversed saturation current density $\overline{J}$ takes the well-known Richardson form of [9,10]

$$\overline{J}_R \propto T^2 e^{-(\Phi/k_B T)}, \tag{2}$$

where Φ denotes the magnitude of the Schottky barrier's height. The exponential term $e^{-\Phi/k_B T}$ in Eq. (2) originates from the classical Boltzmann statistics and is universal regardless of the form of the transport electron-energy dispersion, while the $\overline{J} \propto T^2$ current-temperature scaling relation is a signature of the parabolic energy dispersion of the transport electrons.

For materials with nonparabolic energy dispersion [see Figs. 1(a)–1(d) for examples of nonparabolic energy dispersions], the validity of $\overline{J} \propto T^2$ should be verified. Although it is well known that the energy dispersion plays an important role in governing the Schottky transport, the traditional $\overline{J} \propto T^2$ model is still widely used in the vast majority of recent experimental works on Schottky interfaces composed of materials such as MoS_2, black phosphorus, graphene, and few-layer graphene, where the dispersion is highly nonparabolic [4,11–21]. Therefore, there is a need to reformulate the Schottky model in order to uncover the underlying physics in these structures. For monolayer graphene, it was recently reported that $\overline{J}$ has an unconventional form of $\overline{J}_{\mathrm{Dirac}} \propto T^3 e^{-\Phi/k_B T}$ [22]. The $\overline{J}_{\mathrm{Dirac}} \propto T^3$ behavior can be regarded as the *Dirac-Schottky scaling relation* and is a signature of the linear energy dispersion in graphene [23]. As the form of the energy dispersion can crucially affect the scaling, the Schottky transport model has to be reformulated for the Schottky interface made up of nonparabolic dispersions-based materials. The very distinct forms between the Schottky T^2 scaling and the Dirac-Schottky T^3 scaling also prompts

*Corresponding author.
yeesin_ang@sutd.edu.sg
†Corresponding author.
ricky_ang@sutd.edu.sg

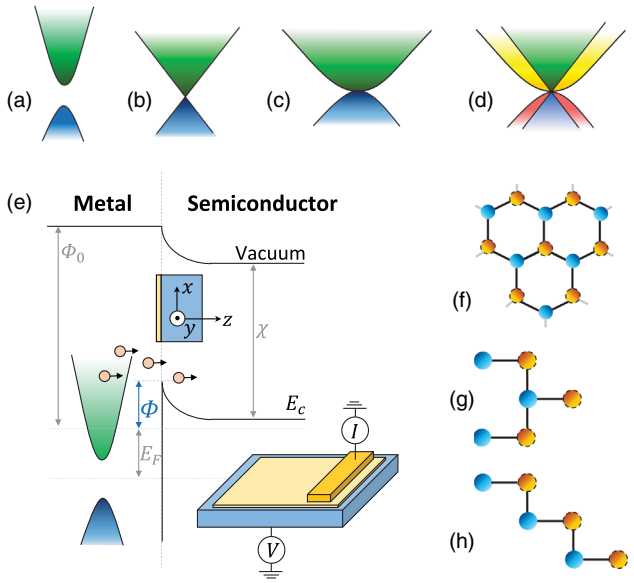

FIG. 1. Nonparabolic energy dispersion and model of Schottky transport. (a) Kane's nonparabolic band, (b) low-energy Dirac cone in graphene, low-energy dispersion of trilayer graphene with (c) *ABA*-stacking and (d) *ABC*-stacking orders, and (e) Schottky transport model in a metal-semiconductor interface. Φ_0 is the work function of the metal, χ is the electron affinity of the semiconductor, and the Schottky barrier is $\Phi = \Phi_0 - \chi$. Inset shows the coordinate system and the geometry of the Schottky interface studied in this work; (f) crystal structure of the graphene layer. Solid (dashed) circle denotes the *A* (*B*) sublattice; (g) *ABA*-stacking order; (h) *ABC*-stacking order.

us to investigate whether the $\overline{J}_R \propto T^2$ and the $\overline{J}_{\text{Dirac}} \propto T^3$ can be connected via a unique energy dispersion that is "intermediate" between parabolic and linear and whether the graphene multilayer follows other forms of unconventional scaling relations.

In this paper, we study the Schottky transport in a narrow-gap semiconductor and in few-layer graphene (FLG) in which the energy dispersion is highly nonparabolic. We show that the Schottky T^2 scaling and the Dirac-Schottky T^3 scaling can be unified under Kane's $\mathbf{k}\cdot\mathbf{p}$ band model for a narrow-gap semiconductor in which the band nonparabolicity is captured by the *nonparabolicity parameter*, γ [24–26]. We obtain a *Kane-Schottky scaling relation* of

$$\overline{J}_{\text{Kane}} \propto (T^2 + 2\gamma k_B T^3) e^{-(\Phi/k_B T)}. \tag{3}$$

The scaling relation exhibits a mixture of T^2 and T^3. Here, γ is responsible for the continuous transition from $\overline{J} \propto T^2$ to $\overline{J} \propto T^3$ scaling. In the case of perfectly parabolic dispersion ($\gamma \to 0$) and perfectly linear dispersion ($\gamma \to \infty$), the scaling becomes $\overline{J} \propto T^2$ and $\overline{J} \propto T^3$, respectively. Thus, the Kane-Schottky scaling relation (SR) is a more general SR that connects the Schottky T^2 scaling and the Dirac-Schottky T^3 scaling. In FLG, we find that the scaling is strongly dependent on the stacking order. For *ABA*-stacked *N*-layer FLG, the Schottky current shows an *N*-fold enhancement due to the presence of *N* conduction subbands. Peculiarly, $\overline{J}^{(N)}_{ABA}$ follows the Dirac-Schottky T^3 scaling universally, regardless of the number of layers. This is in contrast to *ABC* FLG where $\overline{J}^{(N)}_{ABC}$ follows an *N*-dependent scaling of $\overline{J}^{(N)}_{ABC} \propto T^{2/N+1}$. Finally, we show that the *Richardson constant* extracted from the Arrhenius plot disagrees with the actual values by 2 orders of magnitude when an incorrect T^2 scaling is used. This emphasizes the importance of using a correct model when interpreting the experimental data in Schottky devices of nonparabolic energy dispersions.

II. THEORY

The Schottky transport model is shown in Fig. 1(e). $\overline{J}$ is determined by the thermionic emission process for which we briefly describe the formalism here [7,27]. The energy of the emitted electron can be written as $E = E_\perp + E_\parallel$, where $E_\perp$ is the energy component along the emission z direction, and $E_\parallel$ is the energy component that lies in the x-y plane [see inset of Fig. 1(e)]. The electron emission current density is given as

$$\overline{J} = \int_\Phi^\infty N(E_\perp) D(E_\perp) dE_\perp, \tag{4}$$

where $D(E_\perp)$ is the transmission probability, and Φ is the Schottky barrier. For the overbarrier process, $D(E_\perp)$ can be approximated by $D(E_\perp) = \Theta(E_\perp - \Phi)$. The electron supply function $N(E_\perp)$ can be expressed as $N(E_\perp)dE_\perp = dE_\perp \int_{E_\perp}^\infty n(E, E_\perp)dE$, where the electron supply density is

$$n(E, E_\perp)dEdE_\perp = g_{s,v} e v_\perp f(E) \frac{d^3k}{(2\pi)^3}. \tag{5}$$

The group-velocity component along the emission direction is given as $v_\perp = \hbar^{-1} dE_\perp/dk_\perp$, and $f(E)$ is the Fermi-Dirac distribution function. The k-space integration can be rewritten as $d^3k = k_\parallel dk_\parallel d\phi dk_\perp$, where $\mathbf{k}_\parallel = (k_x, k_y)$ denotes the in-plane crystal momentum of the transport electron, $k_\perp$ denotes the out-of-plane momentum component, and $\phi = \tan^{-1} k_y/k_x$. Since the energy of the overbarrier electron is much larger than the Fermi level, the Fermi-Dirac distribution function can be approximated by the Boltzmann distribution function. We can simplify $n(E, E_\perp)dEdE_\perp$ as

$$n(E, E_\perp)dEdE_\perp = dE_\perp \frac{g_{s,v} e}{(2\pi)^3 \hbar} f_{MB}(E) k_\parallel dk_\parallel d\phi, \tag{6}$$

where $f_{MB}(E)$ is the Boltzmann distribution function. In order to complete the $\int(\cdots)dE$ integral in

$N(E_\perp)dE_\perp$, the k-space differentials $k_\parallel dk_\parallel$ need to be converted into $E_\parallel$-space differentials. The $k_\parallel dk_\parallel \to dE_\parallel$ transformation depends on the actual form of the $E_\parallel - k_\parallel$ relation, i.e., the energy dispersion. Therefore, $N(E_\perp)dE_\perp$ contains all of the information about the energy dispersion and plays an important role in determining the form of the Schottky transport current.

III. RESULTS AND DISCUSSION

In this section, we present the Schottky transport models for two classes of nonparabolic energy dispersions: (i) Kane's nonparabolic energy dispersion for the narrow-gap semiconductor and (ii) FLG with ABA stacking and with ABC stacking. For (i), we further consider two related band-structure effects, i.e., Kane's model with band anisotropy and the parabolic model with the higher-order k^4 correction term. The details of the derivation are presented in the appendixes.

A. Kane-Schottky transport model

The electron transport in a narrow-gap semiconductor is well-described by Kane's nonparabolic band model [24,25,28]. As the parabolic energy band is only a good approximation near the conduction-band edge, Kane's model is also an improved band model especially for higher-energy transport electrons [29–31]. Kane's nonparabolic energy dispersion is given as $E_\parallel(1+\gamma E_\parallel) = \hbar^2 k_\parallel^2/2m$, where $\gamma = (1-m/m_0)/E_g$ denotes the nonparabolicity of the dispersion, m_0 is the bare electron mass, and E_g is the magnitude of the band gap. γk_B typically lies in the range of 10^{-4} to 10^{-3} K^{-1} for a sub-electron-volt narrow-gap semiconductor such as PbSe, InAs, InSb, and the topological insulators HgCdTe and Bi_2Te_3 [32–35]. The energy dispersion can be reexpressed as $E_\parallel = (2\gamma)^{-1}(\sqrt{1+4\gamma\hbar^2 k_\parallel^2/2m}-1)$. For small γ, we recover the parabolic dispersion $E_\parallel \propto k_\parallel^2$. For large γ, $E_\parallel(1+\gamma E_\parallel) \approx \gamma E_\parallel^2$, and this yields a linear dispersion of $E_\parallel \propto k_\parallel$. Hence, Kane's model connects the two extreme cases of perfectly parabolic and perfectly linear dispersion via γ. Solving Eqs. (4)–(6) using Kane's nonparabolic energy dispersion, we obtain the *Kane-Schottky-diode equation* as

$$J_{\mathrm{Kane}} = \frac{g_{s,v} e m k_B^2}{4\pi^2\hbar^3}(T^2 + 2\gamma k_B T^3) e^{-(\Phi/k_B T)}(e^{(\mathrm{eV}/\eta k_B T)-1}). \tag{7}$$

The detailed derivation can be found in Appendix A. The reverse saturation current density exhibits a combination of the Schottky T^2 scaling and the Dirac-Schottky T^3 scaling, i.e., $J \propto (T^2 + 2\gamma k_B T^3)$. This finding concludes that the Kane-Schottky model gives a more general scaling relation, as it unifies both Schottky and Dirac-Schottky scaling relations via γ. For the highly parabolic limit, $\gamma \to 0$, and this yields the conventional Schottky T^2 scaling with reverse saturation current density $\overline{J}_{\gamma\to 0} = \mathcal{A}T^2 e^{-(\Phi/k_B T)}$, where $\mathcal{A} = g_{s,v} e m k_B^2/4\pi^2\hbar^3$ is the Richardson constant. In the extremely nonparabolic limit of $\gamma \to \infty$ (i.e., perfectly linear dispersion), the energy dispersion becomes linear in k, i.e., $E_\parallel = \hbar v_F k$ where $v_F \equiv \sqrt{1/2m\gamma}$ and the T^3 term dominates. In this case, Eq. (7) reduces to the Dirac-Schottky form of $J = \mathcal{B}T^3 e^{-(\Phi/k_B T)}$ [22], where $\mathcal{B} = g_{s,v} e k_B^3/4\pi^2\hbar^3 v_F^2$ is the modified Richardson constant in graphene.

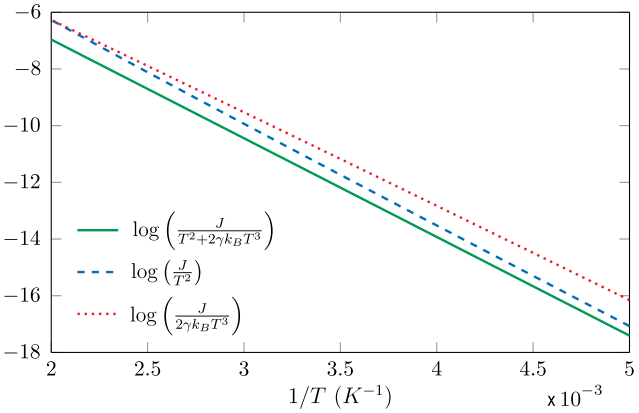

FIG. 2. Arrhenius plot of the Kane-Schottky model using different scaling relation with $\gamma k_B = 10^{-3}$ K^{-1}. Kane-Schotkky, Schottky, and Dirac-Schottky scaling relations are denoted by the solid, dashed, and dotted lines, respectively. The reverse bias is set to $V = -1$ V to ensure current saturation.

The Kane-Schottky-diode model has an implication in the experimental determination of the Richardson constant. In Fig. 2, we generate the Kane-Schottky current density J, with $\Phi = 0.30$ eV and $\eta = 1.1$ for temperatures from 200 to 500 K, and we plot the $1/T$ Arrhenius plot using different scaling relations of (i) $\log[J/(T^2 + 2\gamma k_B T^3)]$, (ii) $\log(J/T^2)$, and (iii) $\log(J/2\gamma k_B T^3)$. Because of the dominating $\exp(\Phi/k_B T)$, scalings (ii) and (iii) are both well fitted by straight lines. The Schottky barrier's heights extracted from the gradients of the linear fit are $\Phi = (0.31, 0.28)$ eV, respectively, for (ii) and (iii). This deviates only slightly from the actual value of 0.30 eV. However, the Richardson constant determined from the y intercepts of the linear fit is $\mathcal{A}_{\mathrm{fit}} = (2.46, 0.0028)\mathcal{A}_0$, respectively, for scalings (ii) and (iii) and disagrees significantly with the actual value $\mathcal{A}_0 \equiv e g_{s,v} m k_B^2/4\pi^2\hbar^3$. This illustrates the importance of using the correct scaling in the Arrhenius plot instead of assuming the conventional T^2 scaling when extracting $\mathcal{A}_{\mathrm{fit}}$ from experimental data.

For completeness, we further demonstrate that the Kane-Schottky scaling relation is robust against band anisotropy and can be similarly obtained by including a higher-order k^4 correction term in the parabolic dispersion. For the former case, we have $E_\parallel(1+\gamma E_\parallel) = \hbar^2 k_x^2/2m_x + \hbar^2 k_y^2/2m_y$, where (m_x, m_y) is the anisotropic effective mass in the x

and y directions, respectively. This energy dispersion yields a Kane-Schottky scaling in the form of

$$\overline{J}_{m_x\neq m_y} = \frac{g_{s,v} e k_B^2 \sqrt{m_x m_y}}{4\pi^2\hbar^3}(T^2 + 2k_B\gamma T^3)e^{-(\Phi/k_BT)}. \quad (8)$$

The latter case represents an alternative approach to account for the band nonparabolicity via a higher-order k^4 term, i.e., $E = \alpha k^2 - \beta k^4$, where $\alpha \equiv \hbar^2/2m$, and β is a small correction factor. In this case, we obtain

$$\overline{J}_{\alpha k^2-\beta k^4} = \frac{g_{s,v} e}{8\pi^2\hbar\sqrt{\beta}}(k_BT)^{3/2}\mathcal{D}_+\left(\sqrt{\frac{\varepsilon_0}{k_BT}}\right)e^{-(\Phi/k_BT)}, \quad (9)$$

where $\mathcal{D}_+(x) = e^{-x^2}\int_0^x e^{t^2}$ is the Dawson integral, and $\varepsilon_0 = \alpha^2/4\beta$ is a characteristic energy. Note that as $\beta \ll \alpha$, $\varepsilon \gg k_BT$ for all practical temperatures. Using the fact that $\mathcal{D}_+(x) \approx 1/2x + 1/4x^3$ for large x, we obtain the Kane-Schottky scaling of

$$\overline{J}_{\alpha k^2-\beta k^4} \approx \frac{g_{s,v} e m^* k_B^2}{4\pi^2\hbar^3}\left(T^2 + \frac{8m^2\beta}{\hbar^4}k_BT^3\right)e^{-(\Phi/k_BT)}. \quad (10)$$

B. Few-layer-graphene Schottky transport model

The electrical properties of FLG are sensitively dependent on the number of layers N and the stacking order [36–48]. FLG with *ABA* and *ABC* stacking are the most thermodynamically stable stacking orders [49]. The energy dispersion of both stacking orders is highly nonparabolic, and this motivates us to develop a nonparabolic Schottky transport model for *ABA* and *ABC* FLG-based Schottky interfaces (see Appendix B for detailed derivations). Ignoring the layer-asymmetry band gap [50,51], the energy dispersion of the n subband of *ABA* FLG is [43,52,53]

$$E_{k_\parallel,n} = t_\perp\cos\left(\frac{\pi n}{N+1}\right) \pm \sqrt{(v_F k_\parallel)^2 + t_\perp^2\cos^2\left(\frac{\pi n}{N+1}\right)}, \quad (11)$$

where $N \geq 3$ is the number of layers, $t_\perp \approx 0.39$ eV is the interlayer hopping parameter [43,49,54], $v_F = 10^6$ m/s is the Fermi velocity, and $n = 1, 2, \ldots, N$ represents each of the $2N$ subbands. $\overline{J}$ can be derived as

$$\overline{J}_{ABA}^{(N)} = N \times \frac{e g_{s,v} k_B^3}{4\pi^2\hbar^3 v_F^2} T^3 e^{-(\Phi/k_BT)}. \quad (12)$$

The Schottky current exhibits an N-fold enhancement and a universal Dirac-Schottky T^3 scaling for all N. The N-fold enhancement can be explained by the presence of N conduction subbands [54]. The N-independent T^3 scaling is a rather surprising result. As the *ABA* FLG contains multiple nonparabolic subbands, one would expect a mixture of T^2 and T^3 terms in the Schottky current equation. However, we find that the T^2 term generated by the $j < N$ subband is exactly canceled out by that of the $(N - j)$ subband (where $j \neq N/2$ is a positive integer). This mutual cancellation leads to the universal Dirac-Schottky T^3 scaling in *ABA* FLG regardless of the number of layers N.

In the case of *ABC* FLG, the low-energy two-band effective tight-binding model [42,52,55] gives an energy dispersion of $E_\parallel = (\hbar v_F)^N/t_\perp^{N-1}k_\parallel^N$. We obtain

$$\overline{J}_{ABC}^{(N)} = \frac{\Gamma(2/N)}{N}\left(\frac{t_\perp}{k_B}\right)^{2-(2/N)}\frac{e g_{s,v} k_B^3}{4\pi^2\hbar^3 v_F^2}T^{(2/N)+1}e^{-(\Phi/k_BT)}, \quad (13)$$

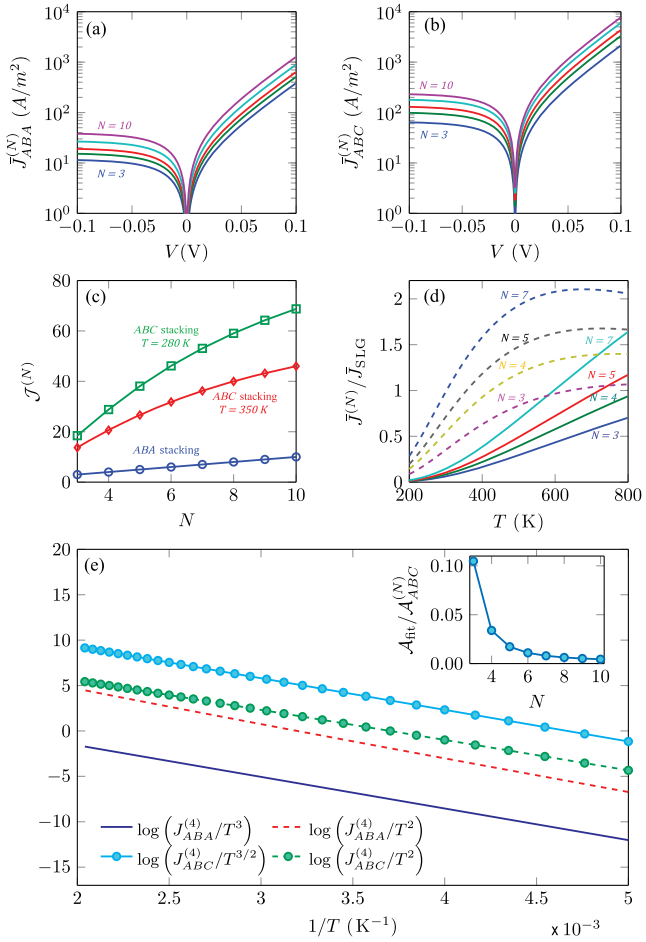

FIG. 3. Schottky transport in few-layer graphene with *ABA*- and *ABC*-stacking orders. *J*-*V* characteristics of (a) *ABA* stacking, (b) *ABC* stacking at $T = 300$ K and $\eta = 1.1$ with for $N = (3, 4, 5, 7, 10)$, (c) the N dependence of the normalized Schottky current, and (d) the temperature dependence of $\bar{J}^{(N)}/\bar{J}_{\text{Dirac}}$. Solid (dashed) lines denote *ABA* (*ABC*) stacking; (e) Arrhenius plot of tetralayer graphene ($N = 4$). The inset shows the N dependence of $\mathcal{A}_{\text{fit}}/\mathcal{A}_{ABC}^{(N)}$.

TABLE I. Summary of the reverse saturation currents and the current-temperature scaling relations for the Schottky transport model of nonparabolic energy dispersions. Note that $e^{-(\Phi/k_BT)}$ is omitted for simplicity.

Energy dispersion	Reverse saturation current	Scaling relation
$E_\parallel(1+\gamma E_\parallel)=(\hbar^2k_\parallel^2/2m)$	$\bar{J}_{\rm Kane}=(g_{s,v}emk_B^2/4\pi^2\hbar^3)(T^2+2\gamma k_BT^3)$	$T^2+2\gamma k_BT^3$
$E_\parallel(1+\gamma E_\parallel)=(\hbar^2k_x^2/2m_x)+(\hbar^2k_y^2/2m_y)$	$\bar{J}_{\rm anisotropy}=(g_{s,v}e\sqrt{m_xm_y}/4\pi^2\hbar^3k_B^2)(T^2+2k_B\gamma T^3)$	$T^2+2\gamma k_BT^3$
$E_\parallel=(\hbar^2k_\parallel^2/2m)-\beta k_\parallel^4$	$\bar{J}_{\alpha k^2-\beta k^4}=(g_{s,v}emk_B^2/4\pi^2\hbar^3)[T^2+(8m^2\beta k_B/\hbar^4)T^3]$	$T^2+(8m^2\beta k_B/\hbar^4)T^3$
$E_{\parallel,n}=t_\perp\cos(\pi n/N+1)$ $\pm\sqrt{(v_Fk)^2+t_\perp^2\cos^2(\pi n/N+1)}$	$\bar{J}_{ABA}^{(N)}=N\times(eg_{s,v}k_B^3/4\pi^2\hbar^3v_F^2)T^3$	T^3
$E_\parallel=[(\hbar v_F)^N/t_\perp^{N-1}]k_\parallel^N$	$\bar{J}_{ABC}^{(N)}=[\Gamma(2/N)/N](t_\perp/k_B)^{2-(2/N)}(eg_{s,v}k_B^3/4\pi^2\hbar^3v_F^2)T^{(2/N)+1}$	$T^{(2/N)+1}$

where $\Gamma(x)$ is a Gamma function. The Schottky current follows an N-dependent scaling relation of $\bar{J}_{ABC}^{(N)}\propto T^{2/N+1}$ in contrast to ABA FLG. The $J-V$ characteristics of ABA FLG and ABC FLG are plotted, respectively, in Figs. 3(a) and 3(b) for a typical Schottky barrier height of $\Phi=0.5$ eV. In general, the Schottky current increases with N in both stacking orders, and $J_{ABC}^{(N)}$ is about an order of magnitude larger than $J_{ABA}^{(N)}$. In Fig. 3(c), we plot the layer dependence of the normalized Schottky current, i.e., $\mathcal{J}_i\equiv\bar{J}_i^{(N)}(T)/\tilde{J}_0(T)$ for $i=(ABA,ABC)$ where $\tilde{J}_0(T)\equiv eg_{s,v}k_B^3T^3e^{-\Phi/k_BT}/(4\pi^2\hbar^3v_F^2)$. $\mathcal{J}_{AB}$ and $\mathcal{J}_{ABC}$ exhibit distinct forms of N dependence. For ABA FLG, $\mathcal{J}_{ABA}\propto N$ and is temperature independent. In contrast, $\mathcal{J}_{ABA}$ exhibits a *temperature-dependent* nonlinear growth with N. To compare the Schottky transport of FLG with that of the monolayer graphene, we define the following ratio:

$$\frac{\bar{J}_{ABA}^{(N)}}{\bar{J}_{\rm Dirac}}=Ne^{-[\Delta\Phi_{AB}^{(N)}/k_BT]},\tag{14a}$$

$$\frac{\bar{J}_{ABC}^{(N)}}{\bar{J}_{\rm Dirac}}=\frac{\Gamma(2/N)}{N}\left(\frac{t_\perp}{k_BT}\right)^{2-(2/N)}e^{-[\Delta\Phi_{ABC}^{(N)}/k_BT]},\tag{14b}$$

where $\Delta\Phi_i^{(N)}\equiv\Phi_i^{(N)}-\Phi_{\rm SLG}$, $\Phi_i^{(N)}$, and $\Phi_{\rm SLG}$ is the Schottky barrier of i-stacking FLG and of the single-layer-graphene Schottky interface, respectively. For simplicity, we assume that $\Delta\Phi_i^{(N)}$ is the same as the work function difference between monolayer graphene and FLG, which has a typical value of $\Delta\Phi_i^{(N)}\approx0.1$ eV [49,56–58]. The temperature dependence of Eq. (14) is shown in Fig. 3(d) for $N=(3,4,5,7)$. At the lower-temperature regime $T\lesssim400$ K, both $\bar{J}_{ABA}^{(N)}/\bar{J}_{\rm Dirac}$ and $\bar{J}_{ABC}^{(N)}/\bar{J}_{\rm Dirac}$ exhibit similar exponential-like growth with increasing T. Although Schottky devices are not typically operated at $T\gtrsim400$ K, it is interesting to note that $\bar{J}_{ABA}^{(N)}/\bar{J}_{\rm Dirac}$ and $\bar{J}_{ABC}^{(N)}/\bar{J}_{\rm Dirac}$ exhibit contrasting high-temperature dependence. $\bar{J}_{ABA}^{(N)}/\bar{J}_{\rm Dirac}$ maintains the exponential growth with increasing T, while $\bar{J}_{ABC}^{(N)}/\bar{J}_{\rm Dirac}$ exhibits a gradual saturation. This behavior can be traced back to the $\bar{J}_{ABC}^{(N)}/\bar{J}_{\rm Dirac}\propto(1/T)^{2-2/N}$ dependence, which balances out $e^{-\Delta\Phi_{ABA}^{(N)}/k_BT}$ at a sufficiently high temperature.

The Richardson constant for ABA FLG and ABC FLG can be defined, respectively, as $\mathcal{A}_{ABA}^{(N)}\equiv N\mathcal{B}$ and $\mathcal{A}_{ABC}^{(N)}\equiv\Gamma(2/N)(t_\perp/k_B)^{2-2/N}\mathcal{B}/N$. We plot the Arrhenius plot with a representative FLG of $N=4$ in Fig. 3(e) using the actual scaling and the conventional T^2 scaling for comparison. For ABA FLG, $J_{ABA}^{(N=4)}/T^2$ is heavily *up-shifted* by orders of magnitudes with respect to the actual scaling $J_{ABA}^{(N=4)}/T^3$. This is contrary to ABC FLG where $J_{ABC}^{(N=4)}/T^2$ is severely *down-shifted* with respect to $J_{ABC}^{(N=4)}/T^{3/2}$. This immediately suggests that the Richardson constants extracted via the incorrect T^2 scaling can severely deviate from the actual values. For ABA stacking, the Richardson constant fitted via $\log(J_{ABA}^{(N)}/T^2)$, i.e., $\mathcal{A}_{\rm fit}$, yields a ratio of $\mathcal{A}_{\rm fit}/\mathcal{A}_{ABA}^{(N)}=870$ for all N, i.e., a nearly 10^3 overestimation. This extremely high overestimation remains approximately constant for all N due to the universal T^3 scaling in ABA FLG. In the inset of Fig. 3(e), $\mathcal{A}_{\rm fit}/\mathcal{A}_{ABC}^{(N)}$ is plotted for N up to 10 for ABC FLG. The strong N dependence is a consequence of the $T^{2/N+1}$ scaling. For ABC-trilayer graphene, $\mathcal{A}_{\rm fit}$ underestimates $\mathcal{A}_{ABC}^{(N=3)}$ by a factor of approximately 0.1. This underestimation becomes worse and reaches $\mathcal{A}_{\rm fit}/\mathcal{A}_{ABC}^{(N)}\approx10^{-3}$ at $N=10$. In contrast, the extracted Schottky barrier height is not significantly influenced by different scaling relations due to the dominance of $e^{-\Phi/k_BT}$. Typically, $\Phi_{\rm fit}/\Phi_{ABA}^{(N)}\approx1.08$ and $\Phi_{\rm fit}/\Phi_{ABC}^{(N)}\approx0.93$, where $\Phi_{\rm fit}$ is the Schottky barrier height fitted from the Arrhenius plot assuming a T^2 scaling. It should be noted that the good agreement between the T^2 fitted and the actual values of Φ [4,11–18] could misleadingly suggest the conventional T^2 model as a valid model for Schottky interfaces composed of nonparabolic energy dispersions. We summarize the main findings of this article in Table I.

IV. CONCLUSION

In summary, we find that the Schottky transport current in a narrow-gap semiconductor and in FLG exhibits distinct forms of unconventional scaling relations. In practice, although the uncertainties of the Richardson constant extracted from an Arrhenius plot can be effectively reduced by using a Legendre polynomial fitting scheme as outlined in Ref. [59], using an incorrect scaling relation can still lead to a severe misinterpretation of the experimental data, yielding an extracted Richardson constant that differs from the actual value by 2 orders of magnitude. Our results highlight the importance of using the correct scaling relation in order to better understand the physics of Schottky devices based on materials with nonparabolic energy dispersions.

ACKNOWLEDGMENTS

This work is supported by Singapore Ministry of Education T2 Grant No. T2MOE1401 and U.S. Air Force Office of Scientific Research (AFOSR) through the Asian Office of Aerospace Research and Development (AOARD) under Grant No. FA2386-14-1-4020. We thank Kelvin J. A. Ooi, M. Zubair, and S. J. Liang for useful discussions.

APPENDIX A: DERIVATION OF THE KANE-SCHOTKKY MODEL

The nonparabolic Kane energy dispersion is given as [24,26,28]

$$E_\parallel(1+\gamma E_\parallel)=\frac{\hbar^2k_\parallel^2}{2m}, \tag{A1}$$

where γ denotes the nonparabolicity of the band structure. The energy dispersion is a simple quadratic equation in $E_\parallel$ and can be solved to obtain

$$E_\parallel=\frac{\sqrt{1+\frac{4\gamma\hbar^2k_\parallel^2}{2m}}-1}{2\gamma}. \tag{A2}$$

This energy dispersion allows us to write down the following transformation:

$$kdk=\frac{m}{\hbar^2}(1+2\gamma E_k)dE_k. \tag{A3}$$

In this case, the function $n(E,E_\perp)$ is given as

$$\begin{aligned} n(E,E_\perp)dEdE_\perp &= g_{s,v}ev_\perp f(E)\frac{d^3k}{(2\pi)^3}\\ &=\frac{2\pi g_{s,v}e}{(2\pi)^3}f(E)k_\parallel dk_\parallel\frac{1}{\hbar}\frac{dE_\perp}{dk_\perp}dk_\perp\\ &=dE_\perp\frac{g_{s,v}em}{(2\pi)^2\hbar^3}[1+2\gamma(E-E_\perp)]f(E)dE, \end{aligned} \tag{A4}$$

where $v_\perp=\hbar^{-1}dE_\perp/dk_\perp$ is the group-velocity component along the emission direction. Assuming the Boltzmann statistic, i.e., $f(E)=e^{-\Phi/k_BT}$, the electron supply function can be written as

$$\begin{aligned} N(E_\perp)dE_\perp &= dE_\perp\frac{g_{s,v}em}{4\pi^2\hbar^3}\int_{E_\perp}^{\infty}[1+2\gamma(E-E_\perp)]f(E)dE\\ &=dE_\perp\frac{g_{s,v}em}{4\pi^2\hbar^3}(-k_BT)(1+2\gamma k_BT)e^{-(E_\perp/k_BT)}. \end{aligned} \tag{A5}$$

This supply function gives the Kane-Schottky-diode equation as

$$\overline{J}_{\rm Kane}=\frac{g_{s,v}emk_B^2}{4\pi^2\hbar^3}(T^2+2\gamma k_BT^3)e^{-(\Phi/k_BT)}. \tag{A6}$$

The Kane-Schotkky scaling relation exhibits a mixture of T^2 and T^3 behavior. In the extremely nonparabolic case, $\gamma\to\infty$, the energy dispersion becomes

$$E_\parallel=\lim_{\gamma\to\infty}\sqrt{\frac{2}{m\gamma}}\hbar k_\parallel. \tag{A7}$$

By defining $v_F=\sqrt{1/2m\gamma}$, the energy dispersion reduces the graphene's linear dispersion, i.e., $E_\parallel=\hbar v_Fk_\parallel$. Using the fact that $\gamma=(2mv_F^2)^{-1}$, we write

$$\overline{J}_{\rm Kane}=\frac{g_{s,v}ek_B^2}{4\pi^2\hbar^3v_F^2}T^3e^{-(\Phi/k_BT)}, \tag{A8}$$

i.e., the modified Richardson law for graphene [22]. In the other extreme case of $\gamma\to0$, the conventional form of $\overline{J}\propto T^2$ can be obtained. In summary,

$$\overline{J}_{\rm Kane}=\begin{cases}\mathcal{A}T^2e^{-(\Phi/k_BT)}, & \gamma\to0,\\ \mathcal{B}T^3e^{-(\Phi/k_BT)}, & \gamma\to\infty,\end{cases} \tag{A9}$$

where $\mathcal{A}=g_{s,v}emk_B^2/4\pi^2\hbar^3$ and $\mathcal{B}=g_{s,v}ek_B^2/4\pi^2\hbar^3v_F^2$.

1. Anisotropic Kane dispersion

In the presence of anisotropy, Kane's nonparabolic energy dispersion can be written as

$$E_\parallel(1+\gamma E_\parallel)=\frac{\hbar^2k_x^2}{2m_x}+\frac{\hbar^2k_y^2}{2m_y}=\theta(\phi)\frac{\hbar^2k^2}{2m_x}, \tag{A10}$$

where $\theta(\phi)\equiv\cos^2\phi+(m_x/m_y)\sin^2\phi$, (m_x,m_y) are the x- and y-direction electron effective mass and $\mathbf{k}_\parallel=(k_x,k_y)$. Equation (A11) can be solved as

$$E_\parallel=\frac{\sqrt{1+\frac{4\gamma\theta(\phi)\hbar^2k_\parallel^2}{2m}}-1}{2\gamma}, \tag{A11}$$

which leads to the $dk\to dE_\parallel$ relation of

$$k_\parallel dk_\parallel = \frac{1}{\theta(\phi)}\frac{m}{\hbar^2}(1+2\gamma E_\parallel)dE_\parallel. \tag{A12}$$

The supply function density then becomes

$$\begin{aligned} &n(E,E_\perp)dEdE_\perp \\ &= dE_\perp \frac{g_{s,v}em_x}{(2\pi)^3\hbar^3}[1+2\gamma(E-E_\perp)] \\ &\quad\times f(E)dE\int_0^{2\pi}\left(\cos^2\phi+\frac{m_x}{m_y}\sin^2\phi\right)^{-1}d\phi. \end{aligned} \tag{A13}$$

The angular integration has a closed form solution of

$$\int_0^{2\pi}\left(\cos^2\phi+\frac{m_y}{m_x}\sin^2\phi\right)^{-1}d\phi = 2\pi\sqrt{\frac{m_y}{m_x}}. \tag{A14}$$

Therefore,

$$\begin{aligned} &n(E,E_\perp)dEdE_\perp \\ &= dE_\perp \frac{g_{s,v}e\sqrt{m_xm_y}}{(2\pi)^2\hbar^3}[1+2\gamma(E-E_\perp)]f(E)dE. \end{aligned} \tag{A15}$$

This is identical to the electron supply function of the isotropy band except that the effective mass m is replaced by the term $\sqrt{m_xm_y}$ in the prefactor. Finally, the emission current density can be determined as

$$\overline{J}_{\text{anisotropy}} = \mathcal{C}(T^2+2k_B\gamma T^3)e^{-(\Phi/k_BT)}, \tag{A16}$$

where $\mathcal{C}\equiv g_{s,v}e\sqrt{m_xm_y}/4\pi^2\hbar^3k_B^2$ is the modified *anisotropic* Richardson constant.

2. Parabolic dispersion with a higher-order k^4 term

Beyond the parabolic band approximation, a higher-order term can be included to account for the nonparabolicity of the band structure at energy far away from the conduction-band edge [30]. In this case, the general form of the energy dispersion can be written as $E_\parallel = \alpha k_\parallel^2 - \beta k_\parallel^4$, where $\alpha = \hbar^2/2m$, and β is a small correction factor. For this energy dispersion, we have

$$k_\parallel dk_\parallel = \frac{dE_\parallel}{2\sqrt{\alpha^2-4\beta E_\parallel}}. \tag{A17}$$

This relation gives the supply function density of

$$n(E,E_\perp)dEdE_\perp = \frac{1}{8\pi^2\hbar}\frac{eg_{s,v}f(E)}{\sqrt{\alpha^2-4\beta(E-E_\perp)}}dEdE_\perp, \tag{A18}$$

and, hence,

$$N(E_\perp)dE_\perp = dE_\perp\frac{eg_{s,v}}{8\pi^2\hbar}\int_{E_\perp}^{\varepsilon_0+E_\perp}\frac{e^{-(E/k_BT)}}{\sqrt{\alpha^2-4\beta(E-E_\perp)}}. \tag{A19}$$

Note that $E_\parallel$ has an unphysical band turning at energy $\varepsilon_0 = \alpha^2/4\beta$. Hence, the upper limit of $\int dE_\parallel$ is set to ε_0. When converting $\int dE_\parallel \to \int dE$, the upper integration limit becomes $\varepsilon_0 + E_\perp$ since $E = E_\perp + E_\parallel$. The integral can be solved analytically as

$$\begin{aligned} N(E_\perp)dE_\perp &= \frac{dE_\perp}{2}\sqrt{\frac{\pi}{\beta}}(k_BT)^{1/2}e^{-(\varepsilon_0/k_BT)}erfi \\ &\quad\times\left(\sqrt{\frac{\varepsilon_0}{k_BT}}\right)e^{-(E_\perp/k_BT)}, \end{aligned} \tag{A20}$$

where $erfi(x)$ is the *imaginary error function*. Finally, we obtain

$$\overline{J}_{\alpha k^2-\beta k^4} = \frac{e}{2}\sqrt{\frac{\pi}{\beta}}(k_BT)^{3/2}e^{-\frac{\varepsilon_0}{k_BT}}erfi\left(\sqrt{\frac{\varepsilon_0}{k_BT}}\right)e^{-(\Phi/k_BT)}. \tag{A21}$$

Using the identity $e^{-x^2}erfi(x) = (2/\sqrt{\pi})\mathcal{D}_+(x)$, where $\mathcal{D}_+(x)\equiv e^{-x^2}\int_0^x e^{t^2}dt$ is the Dawson integral, the current density can be rewritten as

$$\overline{J}_{\alpha k^2-\beta k^4} = \frac{g_{s,v}e}{8\pi^2\hbar\sqrt{\beta}}(k_BT)^{3/2}\mathcal{D}_+\left(\sqrt{\frac{\varepsilon_0}{k_BT}}\right)e^{-(\Phi/k_BT)}. \tag{A22}$$

In the limit of $\varepsilon_0 \gg k_BT$,

$$\begin{aligned} \overline{J}_{\alpha k^2-\beta k^4} &= \frac{g_{s,v}e}{8\pi^2\hbar\sqrt{\beta}}(k_BT)^{3/2} \\ &\quad\times\left[\frac{1}{2}\left(\frac{k_BT}{\varepsilon_0}\right)^{1/2}+\frac{1}{4}\left(\frac{k_BT}{\varepsilon_0}\right)^{3/2}\right]e^{-(\Phi/k_BT)}, \end{aligned} \tag{A23}$$

where the identity of $\mathcal{D}_+(x)\approx 1/2x + 1/4x^3 + \cdots$ for large x is used. Replacing $\alpha = \hbar^2/2m$, we obtain the final form of

$$\overline{J}_{\alpha k^2-\beta k^4} = \frac{g_{s,v}em^*}{4\pi^2\hbar^3}\left[(k_BT)^2+\frac{8m^2\beta}{\hbar^4}(k_BT)^3\right]e^{-(\Phi/k_BT)}. \tag{A24}$$

APPENDIX B: SCHOTTKY MODEL IN FEW-LAYER GRAPHENE

We now derive the reverse saturation current in FLG. FLG can be stacked according to two stacking orders:

(i) Bernal *ABA* stacking and (ii) rhombohedral *ABC* stacking [40,52,53,55]. Experimentally, it was shown that the *ABC* staking made up of 15% of the total area of mechanically exofoliated tri- and tetralayer graphene [60]. For chemically grown graphene multilayer in SiC substrate, *ABC* stacking is the dominant configuration [61]. For completeness, FLG of both *ABA* and *ABC* stacking is considered.

1. *ABA*-stacked few-layer graphene

For *ABC*-stacked FLG, we rewrite the energy dispersion in Eq. (11) of the main text as

$$E_{\parallel,n} = \frac{1 \pm \sqrt{\gamma_{N,n}^2 \hbar^2 v_F^2 k_{\parallel,n}^2 + 1}}{\gamma_{N,n}}, \tag{B1}$$

where $\gamma_{N,n} \equiv [t_\perp \cos(\pi n/N+1)]^{-1}$. Hence,

$$k_{\parallel,n} dk_{\parallel,n} = \frac{\gamma_{N,n} E_{\parallel,n} - 1}{\gamma_{N,n} \hbar^2 v_F^2} dE_{\parallel,n}. \tag{B2}$$

The supply function due to electrons from the n subband is given as

$$N^{(n)}(E_\perp) dE_\perp = dE_\perp \frac{e g_{s,v}}{4\pi^2 \hbar^3 v_F^2} \left[(k_B T)^3 - \frac{(k_B T)^2}{\gamma_{N,n}} \right] e^{-(E_\perp/k_B T)}. \tag{B3}$$

The reverse saturation current density can be calculated as

$$\begin{aligned} \overline{J}_{ABA}^{(N)} &= \sum_{n=1}^{N} \int_{\Phi_{ABA}^{(N)}}^{\infty} N^{(n)}(E_\perp) dE_\perp \\ &= \frac{e g_{s,v}}{4\pi^2 \hbar^3 v_F^2} \sum_{n=1}^{N} \\ &\quad \times [(k_B T)^3 - t_\perp \cos(\pi n/N+1)(k_B T)^2] e^{-(\Phi_{ABA}^{(N)}/k_B T)}. \end{aligned} \tag{B4}$$

Note that the cosine term in the square bracket follows the following identity

$$\cos\left(\frac{j\pi}{k}\right) = -\cos\left(\frac{N-j}{k}\pi\right), \tag{B5}$$

where j is a positive integer with $2j \neq N$ and $j < N$. Therefore, the summation over all n results in the mutual cancellation of the T^2 terms in the square bracket in the second line of Eq. (B4). This mutual cancellation leads to the following *total* reverse saturation current of

$$\overline{J}_{ABA}^{(N)} = N \times \frac{e g_{s,v} k_B^3}{4\pi^2 \hbar^3 v_F^2} T^3 e^{-(\Phi_{ABA}^{(N)}/k_B T)}. \tag{B6}$$

2. *ABC*-stacked few-layer graphene

For *ABC*-stacked N-layer graphene with $N \geq 2$, the low-energy two-band effective Hamiltonian can written as [52]

$$\hat{\mathcal{H}}_{\mathbf{k}} = -\frac{(\hbar v_F)^N}{t_\perp^{N-1}} \begin{pmatrix} 0 & k_-^N \\ k_+^N & 0 \end{pmatrix}, \tag{B7}$$

where $k_\pm = k_x \pm i k_y$. The basis of $\hat{\mathcal{H}}_{\mathbf{k}}$ is composed of the sublattices in the outermost layers, i.e., $(\phi_{A_1}, \phi_{B_N})^T$, since they are responsible for the low-energy dynamics. By diagonalizing $\hat{\mathcal{H}}_{\mathbf{k}}$, the energy dispersion is found to be $E_\parallel = \alpha_N k_\parallel^N$, where $\alpha_N \equiv (\hbar v_F)^{N-1}/t_\perp^{N-1}$. Similarly, the following relation can be determined:

$$k_\parallel dk_\parallel = \frac{1}{N\alpha_N} \left(\frac{E_\parallel}{\alpha_N} \right)^{\frac{2}{N}-1}. \tag{B8}$$

Similarly, the electron supply function can be written as

$$N(E_\perp) dE_\perp = dE_\perp \frac{g_{s,v} e}{4\pi^2 \hbar N \alpha_N} \times \int_{E_\perp}^{\infty} dE \left(\frac{E - E_\perp}{\alpha_N} \right)^{\frac{2}{N}-1} e^{-(E/k_B T)}. \tag{B9}$$

The integral can be analytically solved in terms of an incomplete Gamma function, i.e.,

$$\begin{aligned} &\int_{E_\perp}^{\infty} dE \left(\frac{E - E_\perp}{\alpha_N} \right)^{\frac{2}{N}-1} e^{-(E/k_B T)} \\ &\quad = -\alpha_N^{1-(2/N)} (k_B T)^{(2/N)} \Gamma\left(\frac{2}{N}\right) e^{-(E_\perp/k_B T)}. \end{aligned} \tag{B10}$$

Finally, the current density is found to be

$$\overline{J}_{ABC}^{(N)} = \frac{e g_{s,v} k_B^3}{4\pi^2 \hbar^3 v_F^2} \frac{(t_\perp k_B)^{2-(2/N)}}{N} \Gamma\left(\frac{2}{N}\right) T^{\frac{2}{N}+1} e^{-(\Phi_{ABC}^{(N)}/k_B T)}. \tag{B11}$$

[1] A. K. Geim and I. V. Grigorieva, van der Waals heterostructures, Nature (London) **499**, 419 (2013).

[2] Y. Xu, C. Cheng, S. Du, J. Yang, B. Yu, J. Luo, W. Yin, E. Li, S. Dong, P. Ye, and X. Duan, Contacts between two- and three-dimensional materials: Ohmic, Schottky, and *p-n* heterojunctions, ACS Nano **10**, 4895 (2016).

[3] D.-S. Tsai, K.-K. Liu, D.-H. Lien, M.-L. Tsai, C.-F. Kang, C.-A. Lin, L.-J. Li, and J.-H. He, Few-layer MoS_2 with high broadband photogain and fast optical switching for use in harsh environments, ACS Nano **7**, 3905 (2013).

[4] H. Yang, J. Heo, S. Park, H. J. Song, D. H. Seo, K.-E. Byun, P. Kim, I. Yoo, H.-J. Chung, and K. Kim, Graphene

barristor, a triode device with a gate-controlled Schottky barrier, Science **336**, 1140 (2012).
[5] M.-L. Tsai, S.-H. Su, J.-K. Chang, D.-S. Tsai, C.-H. Chen, C.-I. Wu, L.-J. Li, L.-J. Chen, and J.-H. He, Monolayer MoS_2 heterojunction solar cells, ACS Nano **8**, 8317 (2014).
[6] H. S. Lee, S. S. Baik, K. Lee, S.-W. Min, P.-J. Jeon, J. S. Kim, K. Choi, H. J. Choi, J. H. Kim, and S. Im, Metal semiconductor field-effect transistor with MoS_2/conducting NiO_x van der Waals Schottky interface for intrinsic high mobility and photoswitching speed, ACS Nano **9**, 8312 (2015).
[7] S.-D. Liang, *Quantum Tunnelling and Field Electron Emission Theories* (World Scientific, Singapore, 2013).
[8] C. R. Crowell and S. M. Sze, Current transport in metal-semiconductor barriers, Solid State Electron. **9**, 1035 (1966).
[9] O. W. Richardson, The distribution of the molecules of gas in a field of force, with applications to the theory of electrons, Philos. Mag. **28**, 633 (1914); The influence of gases on the emission of electrons and ions from hot metals, Proc. R. Soc. A **91**, 524 (1915); S. Dushman, Electron emission from metals as a function of temperature, Phys. Rev. **21**, 623 (1923).
[10] C. R. Crowell, The Richardson constant for thermionic emission in Schottky barrier diodes, Solid State Electron. **8**, 395 (1965).
[11] C.-C. Chen, M. Aykol, C.-C. Chang, A. F. J. Levi, and S. B. Cronin, Graphene-silicon Schottky diodes, Nano Lett. **11**, 1863 (2011).
[12] C. Yim, N. McEvoy, and G. S. Duesberg, Characterization of graphene-silicon Schottky barrier diodes using impedance spectroscopy, Appl. Phys. Lett. **103**, 193106 (2013).
[13] S. Kim, T. H. Seo, M. J. Kim, K. M. Song, E.-K. Suh, and H. Kim, Graphene-GaN Schottky diodes, Nano Res. **8**, 1327 (2015).
[14] M. Mohammed, Z. Li, J. Cui, and T.-P. Chen, Junction investigation of graphene/silicon Schottky diodes, Nanoscale Res. Lett. **7**, 302 (2012).
[15] S. Shivaraman, L. H. Herman, F. Rana, J. Park, and M. G. Spencer, Schottky barrier inhomogeneities at the interface of few layer epitaxial graphene and silicon carbide, Appl. Phys. Lett. **100**, 183112 (2012).
[16] S. Tongay, M. Lemaitre, X. Miao, B. Gila, B. R. Appleton, and A. F. Hebard, Rectification at Graphene-Semiconductor Interfaces: Zero-Gap Semiconductor-Based Diodes, Phys. Rev. X **2**, 011002 (2012).
[17] Y. An, A. Behnam, E. Pop, and A. Ural, Metal-semiconductor-metal photodetectors based on graphene/*p*-type silicon Schottky junctions, Appl. Phys. Lett. **102**, 013110 (2013).
[18] L. Yu, Y.-H. Lee, X. Ling, E. J. G. Santos, Y. C. Shin, Y. Lin, M. Dubey, E. Kaxiras, J. Kong, H. Wang, and T. Palacios, Graphene/MoS_2 hybrid technology for large-scale two-dimensional electronics, Nano Lett. **14**, 3055 (2014).
[19] S. Das, H.-Y. Chen, A. V. Penumatcha, and J. Appenzeller, High performance multilayer MoS_2 transistors with scandium contacts, Nano Lett. **13**, 100 (2013).
[20] H. Tian, Z. Tan, C. Wu, X. Wang, M. A. Mohammad, D. Xie, Y. Yang, J. Wang, L.-J. Li, J. Xu, and T.-L. Ren, Novel field-effect Schottky barrier transistors based on graphene-MoS_2 heterojunctions, Sci. Rep. **4**, 5951 (2014).
[21] J. Kang, D. Jariwala, C. R. Ryder, S. A. Wells, Y. Choi, E. Hwang, J. H. Cho, T. J. Marks, and M. C. Hersam, Probing out-of-plane charge transport in black phosphorus with graphene-contacted vertical field-effect transistors, Nano Lett. **16**, 2580 (2016).
[22] S.-J. Liang and L. K. Ang, Electron Thermionic Emission from Graphene and a Thermionic Energy Converter, Phys. Rev. Applied **3**, 014002 (2015).
[23] A. H. Castro Neto, F. Guinea, N. M. R. Peres, K. S. Novoselov, and A. K. Geim, The electronic properties of graphene, Rev. Mod. Phys. **81**, 109 (2009).
[24] E. O. Kane, Band structure of indium antimonide, J. Phys. Chem. Solids **1**, 249 (1957).
[25] B. M. Askerov, *Electron Transport Phenomena in Semiconductor* (World Scientific, Singapore, 1994).
[26] E. M. Conwell and M. O. Vassell, High-field transport in *n*-type GaAs, Phys. Rev. **166**, 797 (1968).
[27] R. H. Fowler and L. Nordheim, Electron emission in intense electric fields, Proc. R. Soc. A **119**, 173 (1928).
[28] J. Wu, W. Walukiewicz, W. Shan, K. M. Yu, J. W. Ager III, E. E. Haller, H. Lu, and W. J. Schaff, Effects of the narrow band gap on the properties of InN, Phys. Rev. B **66**, 201403(R) (2002).
[29] C. Jacoboni and L. Reggiani, The Monte Carlo method for the solution of charge transport in semiconductors with applications to covalent materials, Rev. Mod. Phys. **55**, 645 (1983).
[30] T. Ruf and M. Cardona, Nonparabolicity of the conduction band in GaAs, Phys. Rev. B **41**, 10747 (1990).
[31] A. M. Anile and V. Romano, Non parabolic band transport in semiconductors: Closure of the moment equations, Continuum Mech. Thermodyn. **11**, 307 (1999).
[32] C. Pryor, Eight-band calculations of strained InAs/GaAs quantum dots compared with one-, four-, and six-band approximations, Phys. Rev. B **57**, 7190 (1998).
[33] G. Martinez, M. Schluter, and M. J. Cohen, Electronic structure of PbSe and PbTe. I. Band structures, densities of states, and effective masses, Phys. Rev. B **11**, 651 (1975).
[34] G. L. Hansen, J. L. Schmit, and T. N. Casselman, Energy gap versus alloy composition and temperature in $Hg_{1x}Cd_xTe$, J. Appl. Phys. **53**, 7099 (1982).
[35] B. Y. Yavorsky, N. F. Hinsche, I. Mertig, and P. Zahn, Electronic structure and transport anisotropy of Bi_2Te_3 and Sb_2Te_3, Phys. Rev. B **84**, 165208 (2011).
[36] J.-C. Charlier, X. Gonze, and J.-P. Michenaud, First-principles study of the stacking effect on the electronic properties of graphite(s), Carbon **32**, 289 (1994).
[37] S. Yuan, R. Roldan, and M. I. Katsnelson, Landau level spectrum of *ABA*- and *ABC*-stacked trilayer graphene, Phys. Rev. B **84**, 125455 (2011).
[38] C. H. Lui, Z. Li, K. F. Mak, E. Cappelluti, and T. F. Heinz, Observation of an electrically tunable band gap in trilayer graphene, Nat. Phys. **7**, 944 (2011).
[39] K. F. Mak, J. Shang, and T. F. Heinz, Electronic Structure of Few-Layer Graphene: Experimental Demonstration of Strong Dependence on Stacking Sequence, Phys. Rev. Lett. **104**, 176404 (2010).

[40] W. Bao, L. Jing, J. Velasco, Jr., Y. Lee, G. Liu, D. Tran, B. Standley, M. Aykol, S. B. Cronin, D. Smirnov, M. Koshino, E. McCann, M. Bockrath, and C. N. Lau, Stacking-dependent band gap and quantum transport in trilayer graphene, Nat. Phys. **7**, 948 (2011).

[41] W. Zhu, V. Perebeinos, M. Freitag, and P. Avouris, Carrier scattering, mobilities, and electrostatic potential in monolayer, bilayer, and trilayer graphene, Phys. Rev. B **80**, 235402 (2009).

[42] F. Guinea, A. H. Castro Neto, and N. M. R. Peres, Electronic properties of stacks of graphene layers, Solid State Commun. **143**, 116 (2007).

[43] F. Guinea, A. H. Castro Neto, and N. M. R. Peres, Electronic states and Landau levels in graphene stacks, Phys. Rev. B **73**, 245426 (2006).

[44] Y. Henni, H. P. Ojeda Collado, K. Nogajewski, M. R. Molas, G. Usaj, C. A. Balseiro, M. Orlita, M. Potemski, and C. Faugeras, Rhombohedral multilayer graphene: A magneto-Raman scattering study, Nano Lett. **16**, 3710 (2016).

[45] K. S. Kim, A. L. Walter, L. Moreschini, T. Seyller, K. Horn, E. Rotenberg, and A. Bostwick, Coexisting massive and massless Dirac fermions in symmetry-broken bilayer graphene, Nat. Mater. **12**, 887 (2013).

[46] S. H. Jhang, M. F. Craciun, S. Schmidmeier, S. Tokumitsu, S. Russo, M. Yamamoto, Y. Skourski, J. Wosnitza, S. Tarucha, J. Eroms, and C. Strunk, Stacking-order dependent transport properties of trilayer graphene, Phys. Rev. B **84**, 161408(R) (2011).

[47] M. F. Craciun, S. Russo, M. Yamamoto, J. B. Oostinga, A. F. Morpurgo, and S. Tarucha, Trilayer graphene is a semimetal with a gate-tunable band overlap, Nat. Nanotechnol. **4**, 383 (2009).

[48] A. L. Grushina, D.-K. Ki, M. Koshono, A. A. K. Nicolet, C. Faugeras, E. McCann, M. Rotemski, and A. F. Morpurgo, Insulating state in tetralayers reveals an even-odd interaction effect in multilayer graphene, Nat. Commun. **6**, 6419 (2015).

[49] M. Aoki and H. Amawashi, Dependence of band structures on stacking and field in layered graphene, Solid State Commun. **142**, 123 (2007).

[50] E. McCann, Asymmetry gap in the electronic band structure of bilayer graphene, Phys. Rev. B **74**, 161403 (R) (2006).

[51] M. Koshino and E. McCann, Gate-induced interlayer asymmetry in *ABA*-stacked trilayer graphene, Phys. Rev. B **79**, 125443 (2009).

[52] H. Min and A. H. MacDonald, Electronic structure of multilayer graphene, Prog. Theor. Phys. Suppl. **176**, 227 (2008).

[53] M. Koshino and E. McCann, Trigonal warping and Berrys phase $N\pi$ in *ABC*-stacked multilayer graphene, Phys. Rev. B **80**, 165409 (2009).

[54] A. Grüneis, C. Attaccalite, L. Wirtz, H. Shiozawa, R. Saito, T. Pichler, and A. Rubio, Tight-binding description of the quasiparticle dispersion of graphite and few-layer graphene, Phys. Rev. B **78**, 205425 (2008).

[55] F. Zhang, B. Sahu, H. Min, and A. H. MacDonald, Band structure of *ABC*-stacked graphene trilayers, Phys. Rev. B **82**, 035409 (2010).

[56] T. Filleter, K. V. Emtsev, Th. Seyller, and R. Bennewitz, Local work function measurements of epitaxial graphene, Appl. Phys. Lett. **93**, 133117 (2008).

[57] Y.-J. Yu, Y. Zhao, S. Ryu, L. E. Brus, K. S. Kim, and P. Kim, Tuning the graphene work function by electric field effect, Nano Lett. **9**, 3430 (2009).

[58] S. J. Sque, R. Jones, and P. R. Briddon, The transfer doping of graphite and graphene, Phys. Status Solidi A **204**, 3078 (2007).

[59] K. L. Jensen, M. A. Kodis, R. A. Murphy, and E. G. Zaidman, Space charge effects on the current-voltage characteristics of gated field emitter arrays, J. Appl. Phys. **82**, 845 (1997).

[60] C. H. Lui, Z. Li, Z. Chen, P. V. Klimov, L. E. Brus, and T. F. Heinz, Imaging stacking order in few-layer graphene, Nano Lett. **11**, 164 (2011).

[61] W. Norimatsu and M. Kusunoki, Selective formation of *ABC*-stacked graphene layers on SiC(0001), Phys. Rev. B **81**, 161410(R) (2010).